Numerical Simulation of Gas Explosion with Non-uniform Concentration Distribution by Using OpenFOAM

Aobo Yang,[⊥] Yujiao Liu,[⊥] Ke Gao,* Runzhi Li, Qiwen Li, and Shengnan Li

ACCESS | Metrics & More | Article Recommendations

ABSTRACT: Gas explosions in coal mines have occurred occasionally, which may cause casualties and economic losses. In the actual mine roadway, the gas concentration distribution is uneven because the gas density is lower than that of air. Gas explosion characteristics of uneven gas distribution with the concentration gradient in mine roadways were analyzed by using the open-source computational fluid dynamic code OpenFOAM. The flame and pressure characteristics were calculated, and the flame and shock wave propagation laws of the non-uniform gas—air mixture explosion with different concentration gradients were analyzed and compared with the uniform gas—air mixture gas. The results show that when the overall gas concentration is the same, the flame velocity and the pressure growth rate of the uniform gas explosion are lower than those of the non-uniform, but the pressure peaks of both are similar. At the same time, when the initial volume concentration is 10%, the non-uniform gas explosion has the highest flame propagation velocity and peak value. The peak explosion pressure of different concentration gradients is proportional to the initial concentration. The above studies clarified the characteristics of gas—air mixture explosions with concentration gradients and provided theoretical support for the prevention and control of gas explosion disasters.
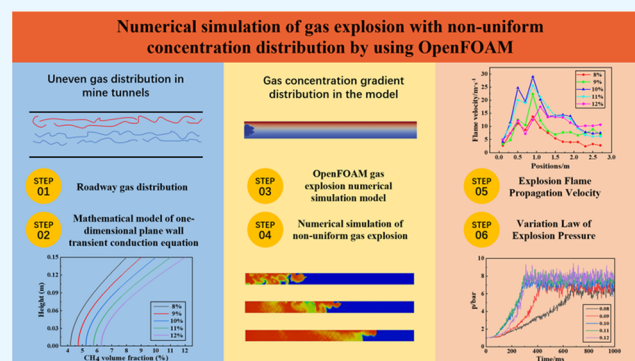
1. INTRODUCTION

Coal energy is an important part of the energy field, supporting the country's economic and social development. However, various combustible gases are inevitably produced during the coal mining process, of which the main component is gas. The disaster caused by the gas explosion is severe.[1−4] Therefore, studying the gas explosion characteristics in a mine roadway is necessary. Before a gas explosion accident, gas accumulation usually occurs, and the accumulated gas stratifies due to lower density with a concentration gradient. So, the study of non-uniform gas explosions with concentration gradients has practical significance.

A gas explosion in the mine roadway is a very complex process, and there are many discussions about the characteristic parameters of the explosion.[5−9] However, previous studies mainly focused on the uniform gas explosion propagation law in mine roadways. Gao et al.[10] did corresponding research on the influence of rock blocks of different sizes on gas explosions. At the same time, in order to study the dynamic pressure effect of the methane—air explosion in the roadway, Zhang et al.[11] carried out the corresponding analysis. Gao et al.[12] also used OpenFOAM to study the influence of low-concentration gas on the gas explosion characteristics of roadways. Regarding the propagation law of the shock wave in the pipeline of the gas explosion, Wang et al.[13] gave their analysis results. Zhou et al.[14]

also conducted a gas explosion experiment by building a model with internal and external obstacles. Regarding the effect of gas concentration on the gas explosion, Cao et al.[15] used Fluent to conduct numerical simulation research on the gas explosion process in pipelines. Yang et al.[16] also carried out corresponding experimental research on the explosion overpressure of gases with different concentrations. At the same time, Xu et al.[17] studied the effect of the gas and air concentration equivalence ratio on the flame propagation in the pipeline. Regarding the process of deflagration to detonation, Cheng et al.[18] provided new experimental evidence supporting the theory of turbulence-enhancement effect on the initiation of a detonation. For the research on the explosion pressure of gases with different concentrations, Wei and Tan[19] analyzed the variation law of the explosion pressure of gases with five different concentrations. Regarding the functional relationship between the gas concentration and the peak explosion pressure, Song[20] gave
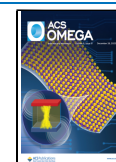
the corresponding experimental research results. Li and Si[21] also studied the explosion pressure and corresponding pressure rise rate of gases with different concentrations through an experimental system. All of the above studies have advanced the gas explosion theory in depth.

However, the gas concentration distribution is often not uniform in the actual mine roadway. The gas concentration is inconsistent everywhere under the influence of the density, and the gas concentration in the mixture is an important factor affecting the explosion characteristics. Therefore, Rui et al.[22] studied the effects of different hydrogen concentration gradients on flame behavior and overpressure through experiments. Huang et al.[23] also studied the joint effect of the vertical concentration gradient and barrier shape on the methane—air explosion characteristics. In order to study the relevant characteristics of the hydrogen—air mixture gas explosion with a concentration gradient, Wang and Wen[24] analyzed the flame propagation velocity and pressure distribution. Karanam et al.[25] also carried out a numerical simulation study on the flame acceleration and DDT of hydrogen—air mixtures.

Some researchers have also contributed to the study of gas explosions. Zhang et al.[26,27] systematically studied the ignition behavior due to shock wave reflections from a variety of shapes and analyzed the effects of the incident shock Mach number (Ma) on the ignition delay times in two reflectors by changing the shock wave intensity. Yang et al.[28] also revealed four flame propagation modes and provided a practical method for differentiating between detonation and deflagration modes. Cao et al.[29,30] also studied the variation law of the explosion pressure of the hydrogen—air mixture in ventilation ducts and the propagation characteristics of the explosion flame of the premixed syngas—air mixture at normal temperature and pressure. At the same time, in order to study the process and mechanism of the gas explosion caused by spontaneous combustion of coal in the goaf, Zhang et al.[31] conducted corresponding simulations. Bi et al.[32] established a three-dimensional numerical model to simulate gas deflagration in pipes of a large length-to-diameter ratio (L/D) and studied the flame propagation and flow field during the deflagration process, as well as the effects of the ignition point and L/D of the pipe on them. Bai et al.[33] used a spherical explosion container to analyze the effect of turbulence on the explosion characteristics of the methane—air mixture. At the same time, Ciccarelli and Dorofeev[34] also studied the unstable combustion phenomenon of combustible mixtures after weak ignition.

This paper constructs a fully enclosed rectangular plane model with a length of 3 m and a height of 0.15 m in view of the uneven distribution of gas in the actual roadway. OpenFOAM was used to study the explosion characteristics of a non-uniform gas—air mixture with a concentration gradient. Under the condition that the diffusion time and other parameters are kept the same, a comparative study of non-uniform gas—air mixture explosions with different concentration gradients is carried out to clarify the characteristics of non-uniform gas—air mixture explosions.

2. NUMERICAL METHODS

Aiming at the flow characteristics of the non-uniform gas—air mixture explosion, the Navier—Stokes equation and the gas—air reaction model are coupled.[35−37] Following the law of mass, energy, and momentum, the mass conservation equation of fluid can be expressed as follows.
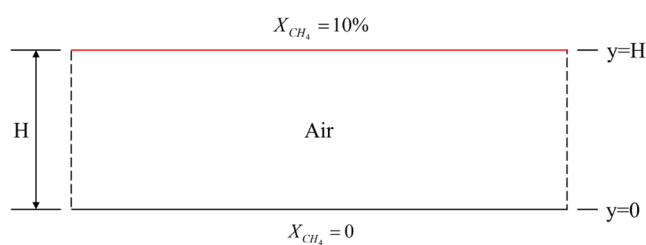

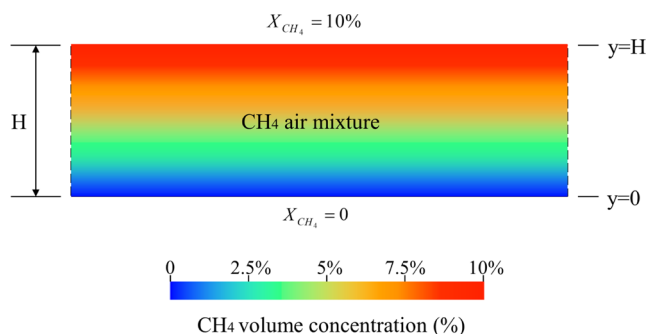Figure 1. Schematic diagram of the initial state.

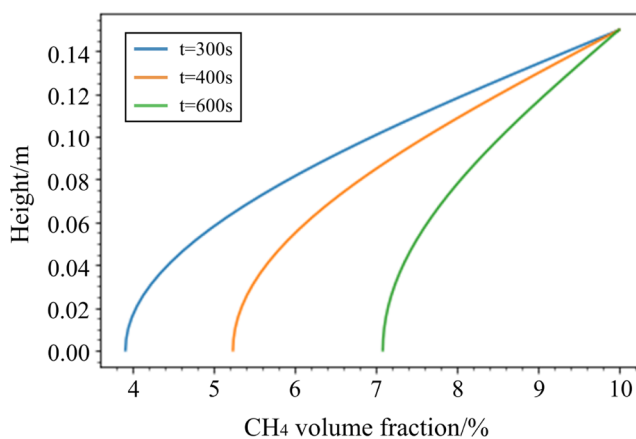Figure 2. Schematic diagram of gas diffusion.

Figure 3. Distribution of the gas volume concentration in the model at the selected time.
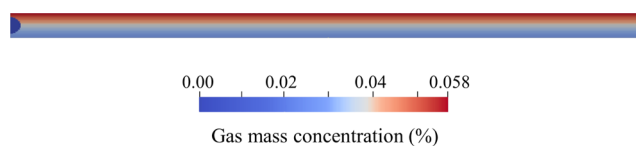

Figure 4. Stratification of non-uniform gas—air mixture.

$$\frac{\partial \rho}{\partial t} + \frac{\partial (\rho u_j)}{\partial x_j} = 0 \tag{1}$$

The momentum conservation equations in each space direction are as follows

$$\frac{\partial (\rho u_i)}{\partial t} + \frac{\partial (\rho u_i u_j)}{\partial x_j} = \frac{\partial \tau_{ij}}{\partial x_j} - \frac{\partial p}{\partial x_i} + \rho g_i \tag{2}$$

where ρ is the density (kg/m^3); t is the time (s); u_i and u_j are the flow velocities (m/s); x_i and x_j are the directions, and τ_{ij} is the shear stress tensor of the Newtonian fluid assumed by Stokes (N/m^2). The expression of τ_{ij} is eq 3, where p is the pressure

(Pa), g_i is the acceleration of gravity (m/s^2), μ is the dynamic viscosity (Pa·s), and δ_{ij} is the Kronecker symbol, $\delta_{ij} = \begin{cases} 1, & i = j \\ 0, & i \neq j \end{cases}$, when i and j = 1, 2, and 3.

$$\tau_{ij} = \mu \left(\frac{\partial u_i}{\partial x_j} + \frac{\partial u_j}{\partial x_i} - \frac{2}{3} \delta_{ij} \frac{\partial u_m}{\partial x_m} \right) \tag{3}$$

The energy conservation equation can be expressed as follows

$$\frac{\partial(\rho e_t)}{\partial t} + \frac{\partial((\rho e_t + p)u_j)}{\partial x_j} = -\frac{\partial q_j}{\partial x_j} + \frac{\partial(\tau_{ij} u_i)}{\partial x_j} \tag{4}$$

where e_t is the overall internal energy (J), $e_t = e + \frac{u_i^2}{2}$. q_j consists of two parts: the heat flow due to heat conduction and the enthalpy flow due to species diffusion.

$$q_j = -K \frac{\partial T}{\partial x_j} + \rho \sum_{k=1}^{N} h_{k,t} \left(-D_k \frac{\partial y_k}{\partial x_j} \right) \tag{5}$$

Where K is the thermal conductivity (W/(m·K)), T is the temperature (K), $h_{k,t}$ is the overall enthalpy of substance k (kJ/kg), D_k is the diffusion coefficient of substance k (m^2/s), y_k is the mass fraction of the substance (%), and N is the quantity of the substance. The conservation equation for the mass of species is as follows

$$\frac{\partial(\rho y_k)}{\partial t} + \frac{\partial(\rho u_j y_k)}{\partial x_j} = \frac{\partial \left(D_k \rho \frac{\partial y_k}{\partial x_j} \right)}{\partial x_j} + \dot{w}_k \tag{6}$$

where $\dot{w}_k$ is the reaction rate of species k (mol/(L·s)) given by eq 7

$$\dot{w}_k = -A\rho C_{CH_4} (C_{O_2})^2 \exp\left(\frac{-E_a}{RT} \right) \tag{7}$$

where A is the pre-exponential factor, E_a is the activation energy (J/mol), C_{CH_4} is the methane concentration (vol %), C_{O_2} is the oxygen concentration (vol %), and R is the universal gas constant (J/(kg·K)).

Equation 7 can be derived from the elementary reaction rate equation and the Arrhenius equation. The object of this study is gas, whose main component is CH$_4$, so the first-order reaction equation is as follows.

$$CH_4 + 2O_2 = CO_2 + 2H_2O \tag{8}$$
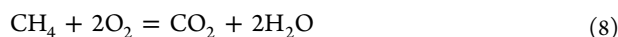
According to chemical kinetics, the basic form of the elementary reaction rate equation can be given as follows

$$v = k C_A{}^a C_B{}^b \tag{9}$$

where v is the reaction rate of the substance, k is the reaction rate coefficient, C_A and C_B are the molar concentrations of substances A and B, respectively, and a and b are the reaction orders. From the given reaction equation of CH$_4$, the reaction orders are $a = 1$ and $b = 2$.

From the Arrhenius equation, the reaction rate coefficient equation can be given as follows

$$k = A e^{-E_a/RT} \tag{10}$$

where k is the reaction rate coefficient, A is the pre-exponential factor/Arrhenius constant, E_a is the activation energy of the

reaction (J/mol), R is the gas constant, and T is the temperature under the absolute temperature scale with the unit being Kelvin (K).

At the same time, according to eq 6, the reaction rate (consumption rate) of CH$_4$ that satisfies eq 6 can be obtained $\dot{w}_k = -\rho v$. It can also be written in the form of eq 7.

The flame propagation is modeled using the reaction progress variable c, where $c = \frac{T - T_f}{T_b - T_f}$. $c = 0$ corresponds to an unburned mixture, and $c = 1$ corresponds to a completely burned mixture. The reaction mass transport equation is as follows

$$\frac{\partial(\rho c)}{\partial t} + \frac{\partial(\rho c u_j)}{\partial x_j} = \frac{\partial \left(\frac{\mu_t}{s_{c_t}} \frac{\partial c}{\partial x_j} \right)}{\partial x_j} + \overline{w}_c \tag{11}$$

where S_{c_t} is the turbulent Schmidt number, μ_t is the turbulent viscosity (Pa·s), and $\overline{w}_c$ is the source term of the reaction process variable. From the Weller model, we know that $\overline{w}_c = \rho S_T |\nabla c| G$, where S_T is the turbulent flame velocity (m/s) and G is a factor ($0 \leq G \leq 1$). The overall reaction rate is $\Omega_c = \int_{-\alpha}^{\alpha} \rho S_T |\nabla c| G \mathcal{F} dx$ (where $\mathcal{F}$ is the flame surface area, m^2).

This study implements the conservation equations by using the finite volume method in the OpenFOAM code. A k-ε model of turbulent flow is used to close the equation,[38] and the HLLC algorithm was proposed based on a density-based solver for the numerical flux. The plane wall's one-dimensional transient conduction equation[39] will also construct the non-uniform gas−air premixed gas.

The governing equation of gas diffusion in the gaseous medium of gas and air is given by eq 12.

$$\frac{\partial(\rho_{mix} Y_{CH_4})}{\partial t} = \frac{\partial}{\partial y} \left(D_{CH_4,mix} \rho_{mix} \frac{\partial}{\partial y} Y_{CH_4} \right) \tag{12}$$

Where ρ is the density (kg/m^3), Y is the mass fraction of the substance, D is the diffusion coefficient (m^2/s), t is the diffusion time (s), and y is the position in the coordinate direction (m).

The volume fraction of species "i" can be obtained in mass fraction using eq 13.

$$X_i = (Y_i/M_i) \bigg/ \left(\sum_i (Y_i/M_i) \right) \tag{13}$$

Where X is the volume fraction of the substance and M is the molecular weight of the substance (kg/kmol).

The input quantities are the input quantities of gas ($\rho_{CH_4,ref}$) and air ($\rho_{air,ref}$) under a normal temperature and one standard atmospheric pressure. The gas−air mixture density is obtained using eq 14. Diffusion coefficients are given by eqs 15 and 16.

$$\rho_{mix} = X_{CH_4} \rho_{CH_4,ref} + X_{air} \rho_{air,ref} \tag{14}$$

$$D_{i,mix} = \frac{0.0018583 \sqrt{T^3 \left(\frac{1}{M_i} + \frac{1}{M_{mix}} \right)}}{p \sigma_{i,mix}^2 \Omega_{i,mix}} \tag{15}$$

$$M_{mix} = X_{CH_4} M_{CH_4} + X_{air} M_{air} \tag{16}$$

Where ($\rho_{CH_4,ref}$) and ($\rho_{air,ref}$) are reference values of gas density.

The schematic diagram of the initial state of gas stratification is shown in Figure 1. In the prefabricated model, the simplified
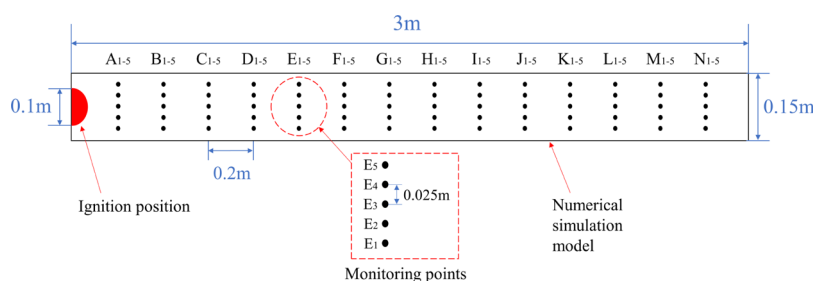
Figure 5. Schematic diagram of the numerical simulation model.

numerical study of one-dimensional diffusion can be carried out, and the analytical solution of the one-dimensional transient conduction equation in the plane wall can be obtained by the numerical method. Meanwhile, Agrawal et al.[40] verified the accuracy of such numerical models and analyzed the errors. It can be calculated that the maximum error of such a numerical model does not exceed 16.5%. In Figure 1, the top plate maintains a gas−air mixture with X = 10% volume concentration, and the initial gas volume concentration in other places is 0. The model governing equation is shown in eq 17.

$$\frac{\partial X_{CH_4}}{\partial t} = D\frac{\partial^2 X_{CH_4}}{\partial y^2} \tag{17}$$

The diffusion coefficient of gas to air is 2.24×10^{-5} m^2/s (fixed value).[41] The bottom and top boundary conditions are expressed by eqs 18 and 19, and the internal initial conditions are expressed by eq 20.

$$X_{CH_4}(H, t) = 0.1 \tag{18}$$

$$\frac{\partial X_{CH_4}(0, t)}{\partial y} = 0 \tag{19}$$

$$X_{CH_4}(y, 0) = 0 \tag{20}$$

Finally, based on the method of solving the one-dimensional transient conduction equation in the plane wall, the analytical solution for the governing eq 17 is given by eq 21, where the variables are given by eqs 22 and 23.

$$\frac{X_{CH_4}(H, t) - 0.1}{0.1} = -A_n \exp(-\lambda_n^2 \tau)\cos\left(\frac{\lambda_n y}{H}\right) \tag{21}$$

$$A_n = \frac{4\sin(\lambda_n)}{2\lambda_n + \sin(2\lambda_n)} \tag{22}$$

$$\lambda_n = (4n + 1)\pi/2 \tag{23}$$

Where n is a constant, H is the overall height of the space (m), and τ is the dimensionless time.

The stratification of the gas concentration caused by molecular diffusion can be described as a one-dimensional mass transfer problem. Figure 2 presents the diffusion diagram illustrating the diffusion state at a specific moment with the initial state depicted in Figure 1. Additionally, Figure 3 illustrates the variation of gas volume concentration with position when the diffusion time are 300, 400, and 600 s.

In this study, when the diffusion time is 400 s, the layering of the gas−air mixture is simulated. The specific non-uniform gas layering in OpenFOAM is shown in Figure 4 (the displayed

concentration value is the mass concentration of the gas). The gas concentration in the figure shows obvious stratification.

3. MODEL CONSTRUCTION AND SIMULATION PROGRAM INTRODUCTION

Figure 5 shows a schematic diagram of the numerical simulation model using the OpenFOAM code. The model uses a planar

Table 1. Input Parameters

| initial conditions	values
p_0	101,325 Pa
T_0	291.18 K
$(u_i)_0$	0 m/s
$(u_j)_0$	0 m/s
Δt	5×10^{-4} s
ρ_{air}	1.29 kg/m^3
ρ_{CH_4}	0.657 kg/m^3

model with length L = 3 m and height H = 0.15 m. Under initial atmospheric temperature and standard atmospheric pressure conditions, a stoichiometric gas−air mixture is filled for the numerical simulation of the gas explosion. Such models have been verified for accuracy and error analysis.[12] The maximum error of its flame speed did not exceed 20.7%. The experimental and simulation results of pressure changes are in good agreement.

The parameters for the simulation model are listed in Table 1. The OpenFAOM numerical model is completely airtight, and the boundary condition is an adiabatic wall. Grid sizes of 2.5, 5, and 10 mm were chosen for grid independence verification to reduce the discretization error and ensure the accuracy of numerical simulation results. Using the monitoring point C_5 as an example (as shown in Figure 6a), the start time of the temperature rise is the same at 5 mm grid size as it is at 2.5 mm grid size. Figure 6b illustrates a significant difference in the pressure change pattern between the 10 mm grid and the 5 mm grid. However, when the grid size is reduced to 5 mm, the pressure growth trend aligns with that of the 2.5 mm grid. Considering the calculation time, a grid size of 5 mm was carried out.

The characteristics of the explosion of a non-uniform gas−air mixture with a concentration gradient are studied by comparing it with the explosion of a uniform gas−air mixture. The concentration gradient was changed by varying the initial concentration in this study, allowing for a systematic analysis of the non-uniform gas−air mixture explosion with different concentration gradients. Therefore, multiple cases will be employed for numerical simulation research to analyze the characteristics of non-uniform gas explosions through comparison. Table 2 shows all of the numerical simulation cases.
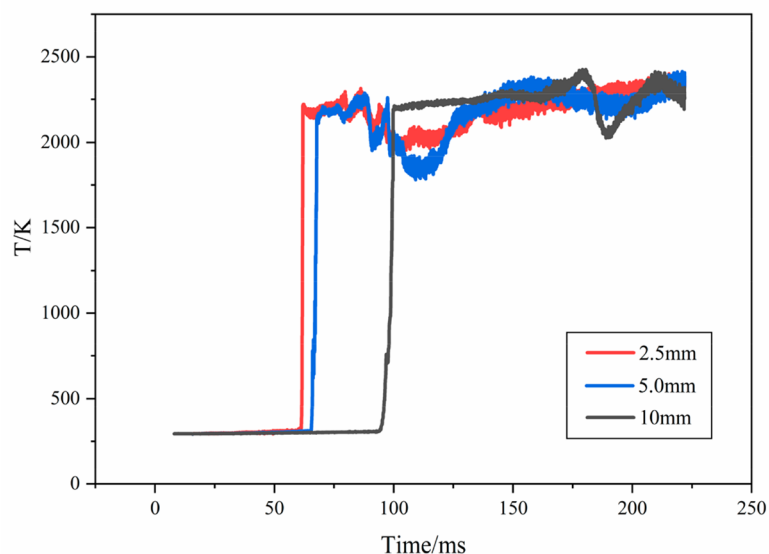
(a) Grid dependence on temperature
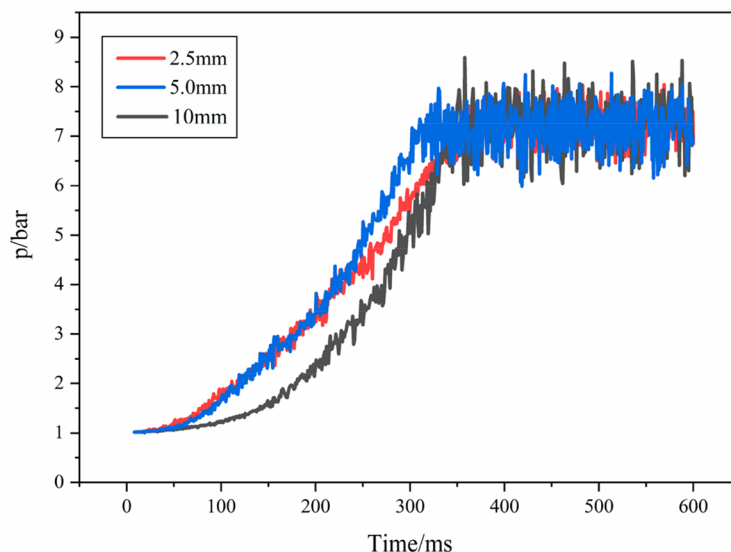

(b) Grid dependence on pressure

Figure 6. Grid independence verification.

**Table 2. Parametric Simulation Details of Different Gas Explosion Cases**

simulation cases	initial concentrations	is it uniform
case 1	10%	no
case 2	6.99%	yes
case 3	8%	no
case 4	9%	no
case 5	11%	no
case 6	12%	no

Case 1 focuses on the explosion of a non-uniform gas−air mixture with a concentration gradient, where the initial volume concentration is 10%. It aims to investigate the fundamental propagation law of the explosion. This paper examines the relationship and distinction between explosions of uniform and non-uniform gas−air mixtures with the same overall gas concentration. Case 2 is numerically simulated, while the other parameters are consistent. Figure 7 illustrates that the overall gas concentration throughout the entire pipe, for a non-uniform gas−air mixture with an initial volume concentration of 10% and a concentration gradient, is 6.99%. Therefore, the entire pipeline is filled with a uniform gas−air mixture with a volume concentration of 6.99%. The numerical simulation results are compared with case 1 to ensure the consistency of the overall gas concentration. The flame and pressure characteristics are also studied. Additionally, numerical simulations were conducted for cases 3−6 to explore the characteristics of gas−air mixture explosions with varying concentration gradients. Keeping the diffusion time ($t = 400$ s) and all other parameters consistent, the initial volume concentration of gas on the upper wall of the pipeline is varied: 8, 9, 11, and 12%. Figure 8
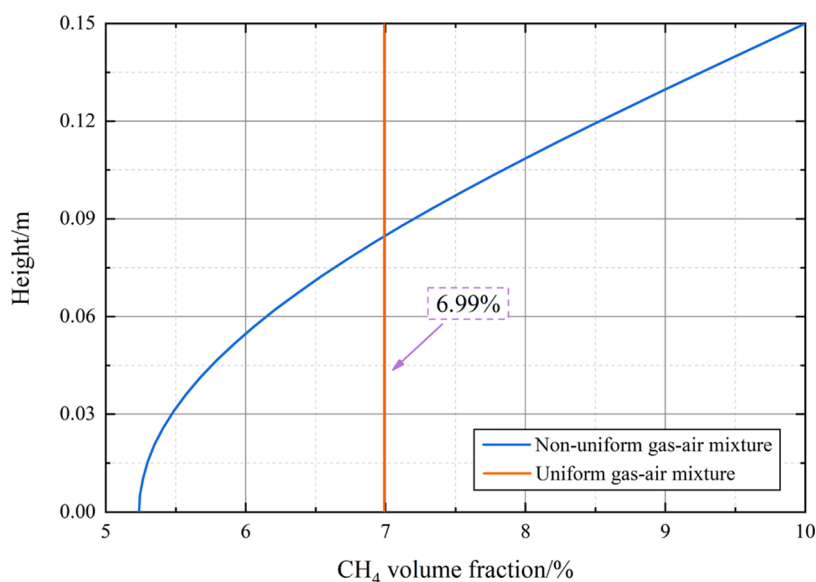
Figure 7. Concentration distribution of uniform and non-uniform gas−air mixtures.
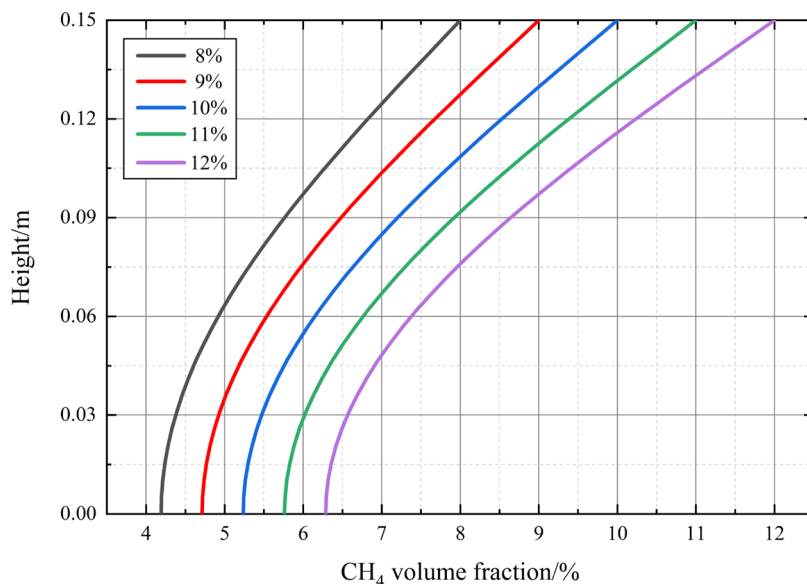
Figure 8. Distribution of the gas volume concentration in different concentration gradients.

illustrates a comparison between the formed concentration gradient and the 10% concentration gradient. Subsequently, a comprehensive comparison was conducted on the simulation results of non-uniform gas explosions with varying concentration gradients, and the characteristics of flame and pressure were analyzed.

4. NUMERICAL SIMULATION RESULTS AND ANALYSIS

4.1. Flame Characteristics of Non-uniform and Uniform Gas−Air Mixture Explosion. *4.1.1. Basic Characteristics of Non-uniform Gas−Air Mixture Explosion Flame.* Figure 9 illustrates the temperature variation over time of the monitoring point (taking $A_1−N_1$ as an example) in case 1. There is a noticeable increase in the temperature in the figure, and the starting time represents the arrival time of the flame front.

Figure 10 depicts the average flame speed for case 1. The average flame speed is calculated using the following equation based on the flame front position versus time[42]

$$v = \frac{x_{i+1} - x_i}{t_{i+1} - t_i} \tag{24}$$

where t_i and t_{i+1} represent the times when the flame front reaches a monitoring point and its subsequent monitoring point, respectively. x_i and x_{i+1} represent the positions of these two adjacent monitoring points, respectively. The average flame speed between two adjacent monitoring points can be calculated to study the non-uniform flame velocity characteristics of a gas−air mixture explosion. Subsequently, $x_{i+1/2}$ represents the position between x_i and x_{i+1}.

The average flame propagation velocity in Figure 10 shows that upon ignition of the gas−air mixture, the sharp increase in temperature and pressure leads to turbulence, which in turn promotes the propagation of the flame. During the initial
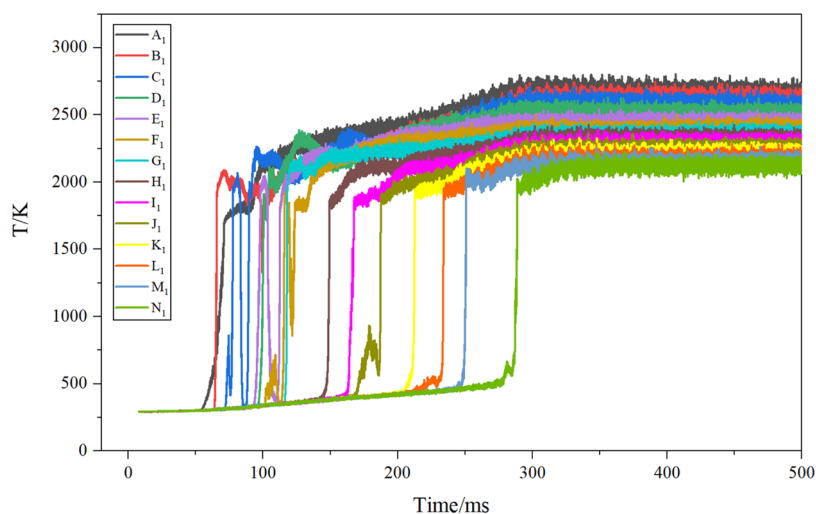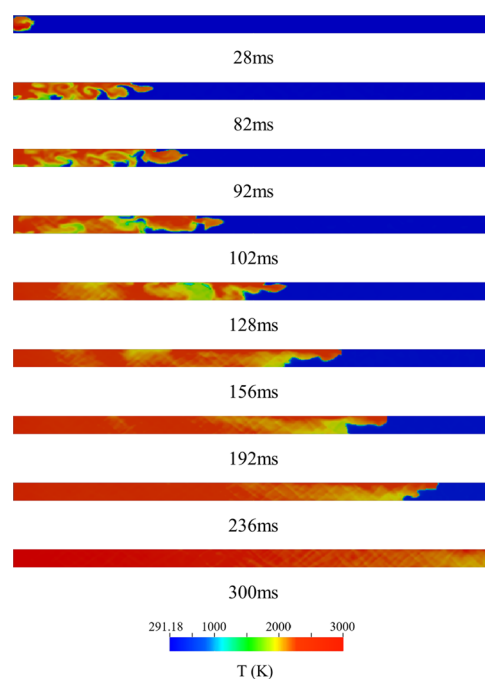
Figure 9. Temperature variation with time of monitoring points A_1-N_1 in case 1.
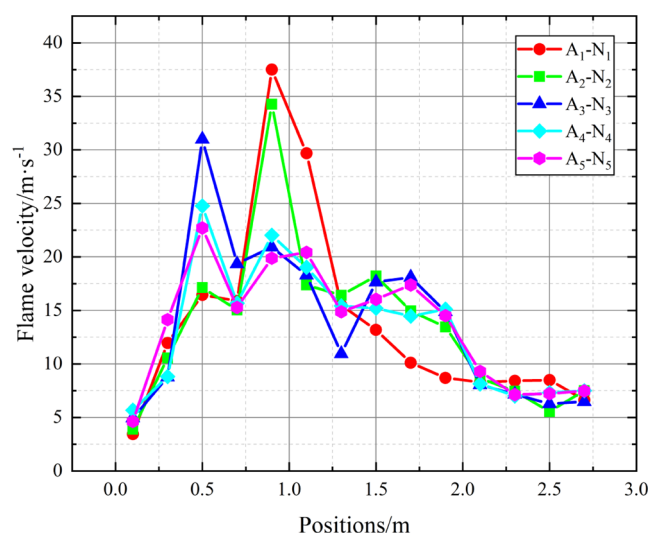
Figure 10. Average flame propagation speed of case 1.

Figure 11. Schematic diagram of case 1 flame shape.

ignition, the gas began to burn gradually, resulting in a flame speed of 5 m/s. As the flame continued to come into contact with the unburned gas−air mixture, the combustion intensified, leading to an increase in the flame speed. Subsequently, the flame speed decreased at 0.7 m, followed by another increase and reaching the peak value. Finally, the flame speed decreased again and stabilized at 7.5 m/s.

As shown in the flame propagation form diagram in Figure 11, due to the non-uniform gas distribution, the flame front spreads close to the upper wall. However, due to the leading shock wave generated by the combustion at the front of the flame, which propagates backward before the flame, it reflects when it touches the end of the pipe and propagates in the opposite direction. When the reflected shock wave meets the flame front, the shock wave will compress the flame, and the speed of the flame will drop accordingly, as can be clearly seen at 0.7 m in Figure 10. Afterward, the compression of the shock wave forces the flame front to compress into the mixture at the bottom. At this time, the increase of the density of the mixture and the increase of the surface area of the flame lead to a sharp rise in the reaction rate of gas and an overall reincrease in the flame speed again. After this, the flame speed gradually decreases and eventually levels off.

It can be seen that although the highest speed of flame propagation appears at the bottom monitoring point, the flame speed of the upper layer is constantly kept between 15 and 25 m/s in the range of 0.5−1.9 m. Therefore, the overall flame propagation speed is still related to the concentration, and the flame propagation speed in the high-concentration area is generally higher than that in the low-concentration area.

4.1.2. Flame Propagation Characteristics of Non-uniform and Uniform Gas−Air Mixture Explosion. Case 2 represents a uniform gas explosion with the same overall gas concentration as case 1. Figure 12 illustrates the shape of the flame propagation. In contrast to case 1, the flame form of the uniform gas explosion is more stable. Since there is no concentration difference in the vertical direction, there is no position gap in the propagation of the flame front. As a result, the flame shape remains consistently flat and propagates steadily backward. Figure 13 depicts the average flame propagation velocity, which exhibits a variation trend similar to that of case 1. Following ignition, the flame
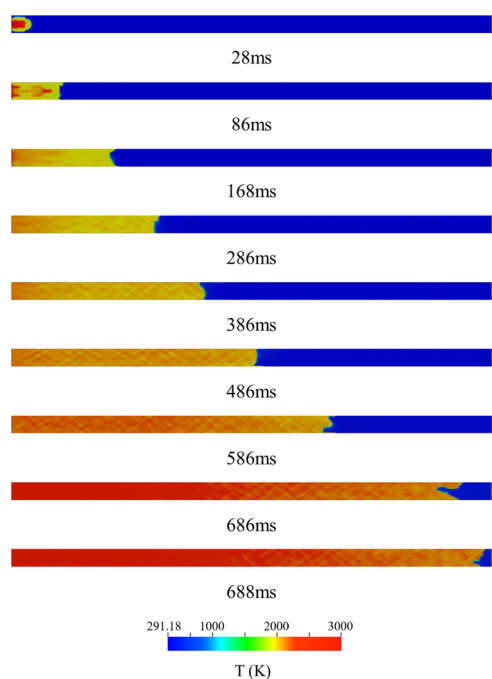
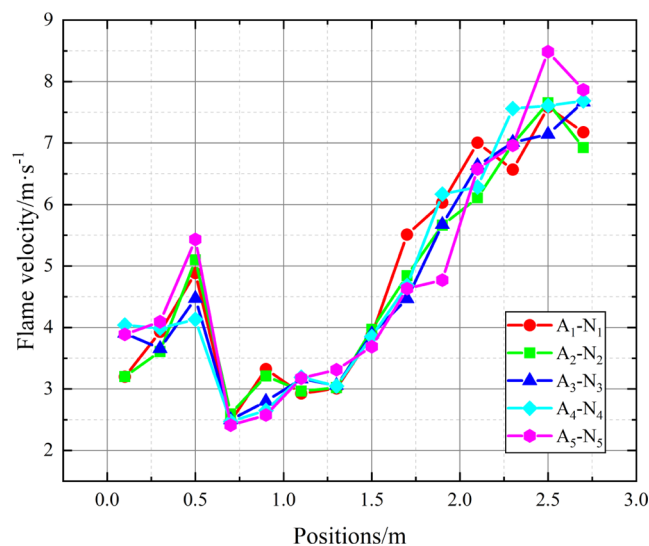**Figure 12.** Schematic diagram of case 2 flame shape.

Figure 13. Average flame propagation velocity of the gas with a uniform concentration.

Figure 14. Flame speeds of non-uniform and uniform gas−air mixture explosions.

propagation velocity initially increases, then decreases, and subsequently increases again before finally stabilizing. Similar to case 1, the leading shock wave generated by the flame is reflected from the end of the pipe. At 0.7 m, the reflected shock wave compresses the flame front, resulting in a reduction in the flame speed. After that, the flame continues to spread, igniting more unburned gas and gradually increasing the flame speed until it stabilized at 7.5 m/s.

Figure 14 illustrates the comparison of the flame speeds between non-uniform and uniform gas−air mixture explosions; the average flame speed of the non-uniform gas−air mixture is 13.7 m/s, and that of uniform is 4.8 m/s. The flame propagation speed of non-uniform gas−air mixtures is higher than that of uniform gas−air mixtures. This is due to the presence of a concentration gradient in the non-uniform gas−air mixture,
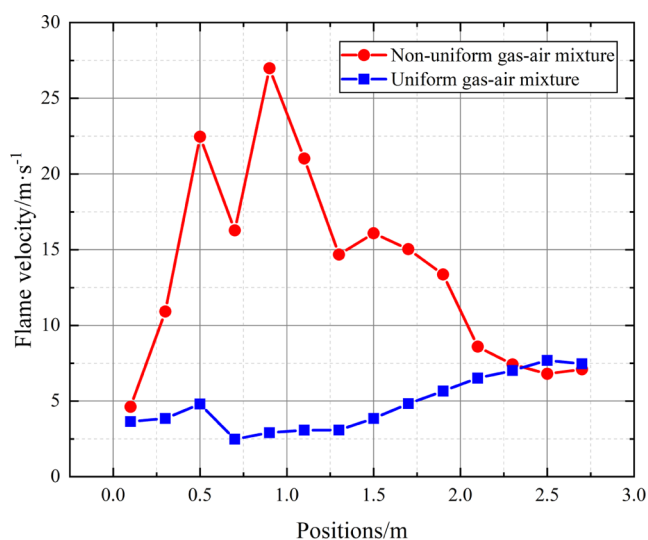
where the gas concentration in the upper layer is higher than the average concentration. As a result, the flame preferentially propagates toward the high-concentration area. Additionally, the gas in the high-concentration area burns more intensely and spreads faster, while the flame speed in the low-concentration area is slower. This causes the flame shape of the non-uniform gas−air mixture to elongate, resulting in a larger surface area. The uniform flame spread exhibits no variation in longitudinal concentration, resulting in a uniform flame shape with a significantly smaller surface area compared to the non-uniform gas−air mixture. Thus, the flame speed of the non-uniform gas−air mixture explosion is higher than the uniform one, which can be attributed to the difference in the flame surface area and gas concentration gradient.

4.1.3. Flame Characteristics of Non-uniform Gas−Air Mixture Explosions with Different Concentration Gradients. The initial concentrations on the upper wall are adjusted in cases 3 and 6 while keeping all other parameters, such as diffusion time, consistent with case 1, in order to create various concentration gradients in the vertical direction. Subsequently, explosion simulations will be conducted for non-uniform gas−air mixtures with different concentration gradients. Figure 15 displays the flame propagation velocity for each concentration gradient. When considering Figure 10, the velocity variation trend of flames resulting from explosions of non-uniform gas−air mixtures with different concentration gradients aligns with that of case 1. In other words, the flame accelerates gradually at the beginning of combustion, followed by a decrease caused by the reflected shock wave. Afterward, the speed continues to increase, reaching the peak value, and then, the flame speed begins to decrease continuously and finally stabilizes. This phenomenon can be explained by the fact that the explosion of non-uniform gas−air mixtures with different concentration gradients has a similar explosion process, and the change of flame propagation speed follows a similar law.

Figure 16 illustrates the comparison of flame speeds with different concentration gradients. The monitoring values represent the average speeds of the monitoring points at various heights within a specific section of the pipeline. The highest flame propagation velocity is observed in the gas−air mixture explosion with an initial concentration of 10% and a
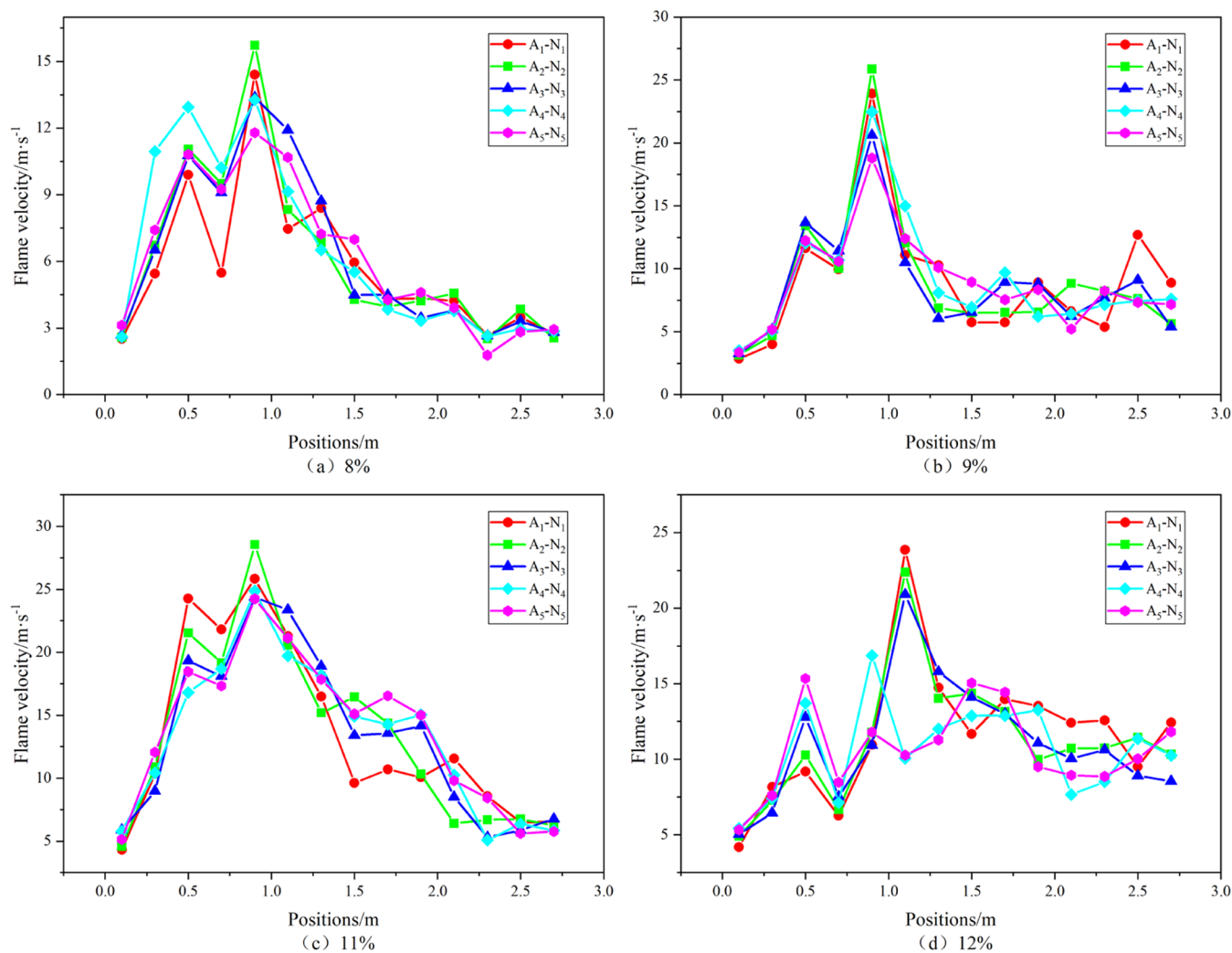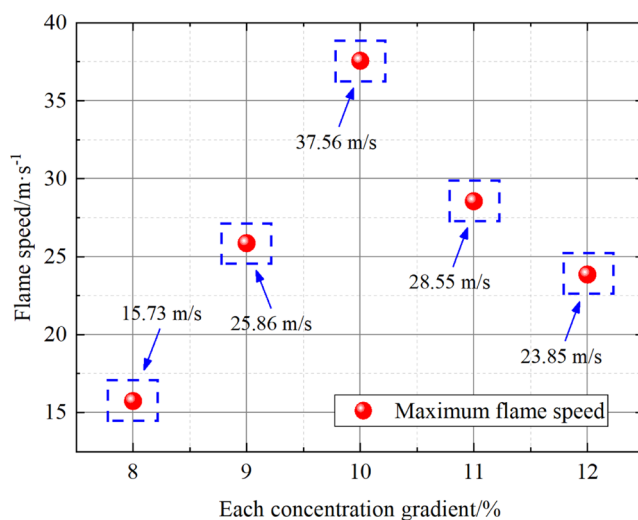
Figure 15. Average flame propagation velocity of different concentration gradients.
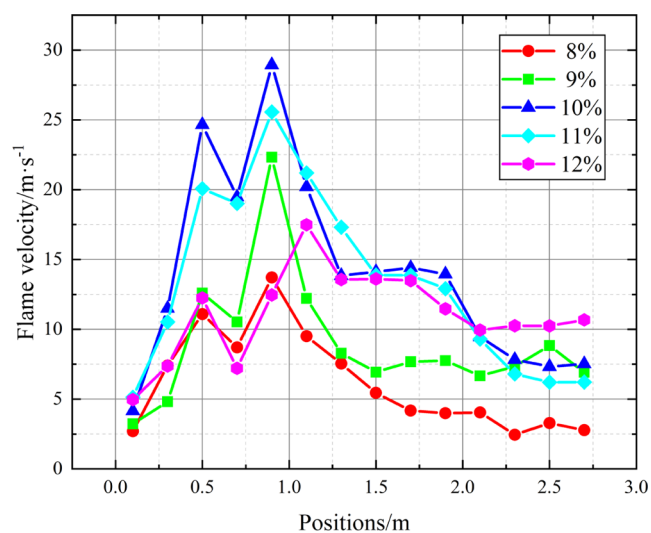
Figure 16. Average flame propagation speeds with different concentration gradients.

Figure 17. Flame speed peaks at different concentration gradients.

concentration gradient. The overall flame propagation velocity gradually decreases as the initial concentration increases or decreases. By considering the flame velocity peaks for each concentration gradient shown in Figure 17, it can be concluded

that the non-uniform gas−air mixture exhibits the highest combustion rate, fastest flame propagation speed, and peak velocity when the initial volume concentration is 10%. As the initial concentration increases or decreases, the flame's overall propagation velocity and peak velocity also decrease.
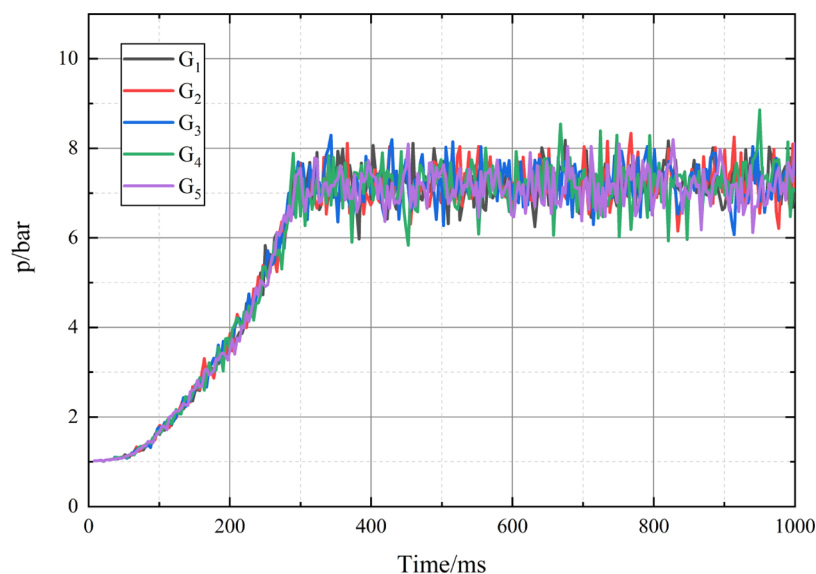
Figure 18. Variation of the explosion pressure of the non-uniform gas−air mixture with time (monitoring points G_1−G_5).
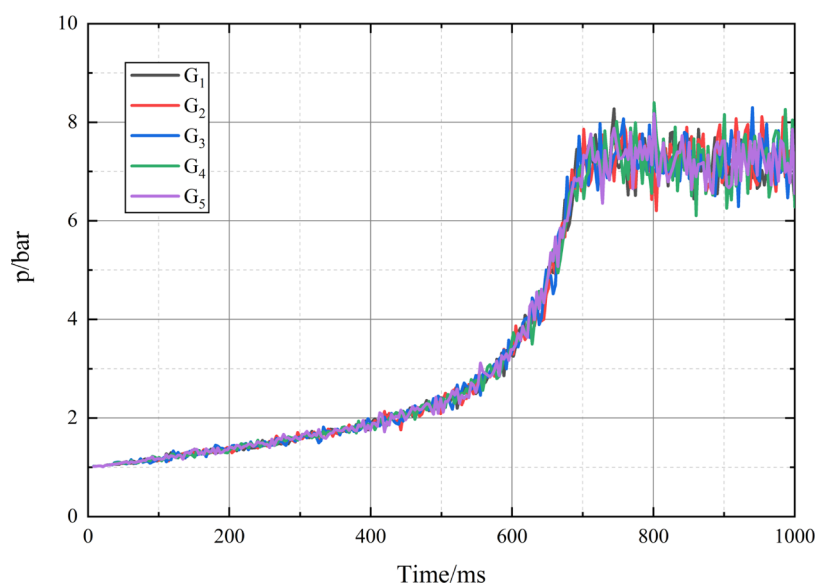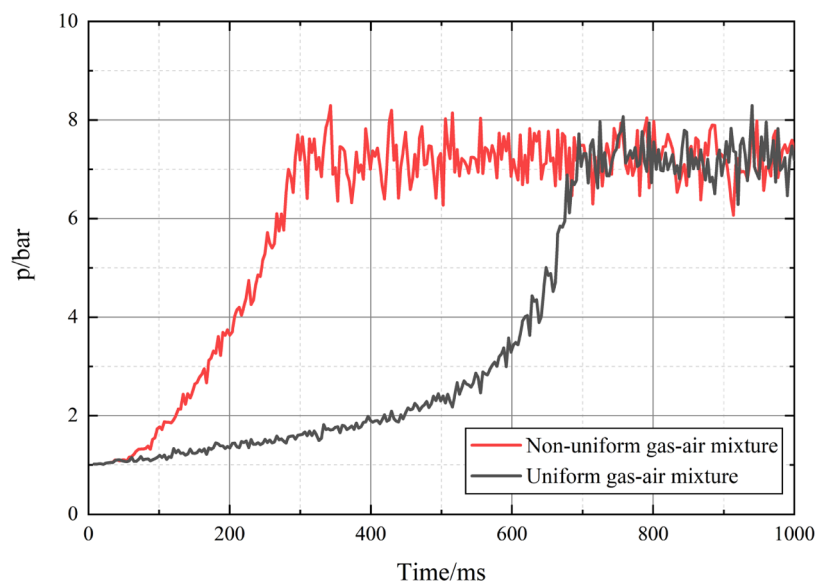

Figure 19. Variation of the explosion pressure of the uniform gas−air mixture with time (monitoring points G_1−G_5).

When the concentration gradient is altered, the magnitude of the flame propagation velocity changes significantly. The non-uniform gas−air mixture explosion with a concentration gradient and initial volume concentration of 10% exhibits the highest overall flame propagation velocity and flame peak velocity. Both the overall propagation and peak velocity decrease as the concentration increases or decreases. Thus, it can be concluded that different concentration gradients have a significant effect on the flame propagation velocity.
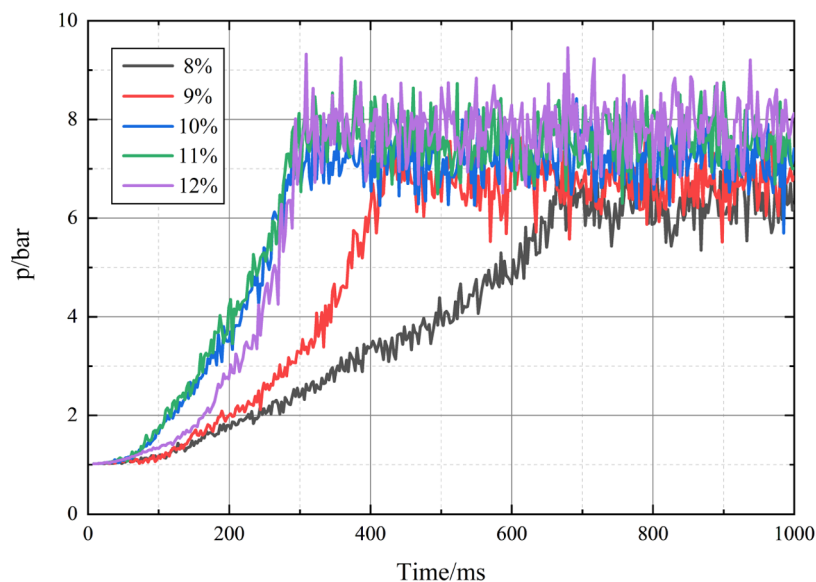
4.2. Explosion Pressure Characteristics of Non-uniform and Uniform Gas−Air Mixtures. *4.2.1. Basic Characteristics of the Explosion Pressure of the Non-uniform Gas−Air Mixture.* The explosion pressure variation image simulated by case 1 can be seen in Figure 18. The monitoring points at different heights but in the same position have the same variation law of explosion pressure and do not change due to the concentration gradient. Therefore, it can be concluded that the change in explosion pressure is independent of the concentration gradient of the non-uniform gas−air mixture. The change

law of explosion pressure is that it rises continuously at first, then reaches the peak value, and finally becomes stable at the peak value. This phenomenon is explained by the fact that after the non-uniform gas−air mixture is ignited, the pressure generated by the restricted flame due to the roadway's height and the wall is the same on the upper and lower walls. The flame shock wave spreads in multiple directions but finally mainly impacts toward the end of the pipeline. As the flame continues to advance, more unburned gas is added to the combustion, making the pressure always maintain an upward trend, then reach a peak, and finally become stable.

4.2.2. Pressure Characteristics of Non-uniform and Uniform Gas−Air Mixture Explosions. The explosion pressure change image simulated by case 2 can be seen in Figure 19. It is similar to the explosion pressure map of case 1. The monitoring points at the same location and heights have the same change trend in explosion pressure. The variation law of the explosion pressure is similar to that shown in Figure 18. It rises continuously, reaches the peak value, and finally becomes stable

Figure 20. Comparison of the explosion pressure of non-uniform and uniform gas−air mixtures.

Figure 21. Comparison of the explosion pressure of non-uniform gas−air mixtures with different concentration gradients.

at the peak value. Combining the non-uniform and uniform pressure comparison chart shown in Figure 20, under the same overall gas concentration, the growth rate of the explosion pressure of the uniform gas−air mixture is much smaller than that of the non-uniform gas−air mixture, the time to reach the pressure peak is also longer, but the pressure peak is essentially the same. This can be explained by the fact that under the same overall concentration, the non-uniform gas−air mixture of case 1 has a concentration gradient, and the gas volume concentration in the upper part of the pipeline is higher than the average concentration. Therefore, the combustion of the gas is more violent, the explosion pressure is higher, and the speed of backward flame propagation is faster. The rate of the explosion pressure rise in the pipeline is also higher. However, although the rate of pressure change is different for cases 1 and 2, the peak pressure is essentially the same because the overall gas concentration and the overall combustible gas are the same.

4.2.3. Explosion Pressure Characteristics of Non-uniform Gas−Air Mixtures with Different Concentration Gradients. The pressure growth changes of each concentration gradient are shown in Figure 21. As shown in the figure, no matter how the concentration gradient changes, the growth trend of the explosion pressure is the same, and the pressure change always rises first and then tends to be stable. When the initial concentration is 10% of the concentration gradient and above, their explosion pressure growth rates are similar and remain at a high level, and they both reach their peak at around 0.3 s. When the initial concentration is reduced to 9 and 8%, the rising rate of the explosion pressure is significantly reduced and the time for the pressure to reach the peak becomes longer. The explosion pressure of the non-uniform gas−air mixture with a concentration gradient at an initial concentration of 9% reaches its peak at 0.42 s, while the explosion pressure of the non-uniform gas−air mixture with a concentration gradient at an initial concentration of 8% reaches the pressure peak at 0.67 s.
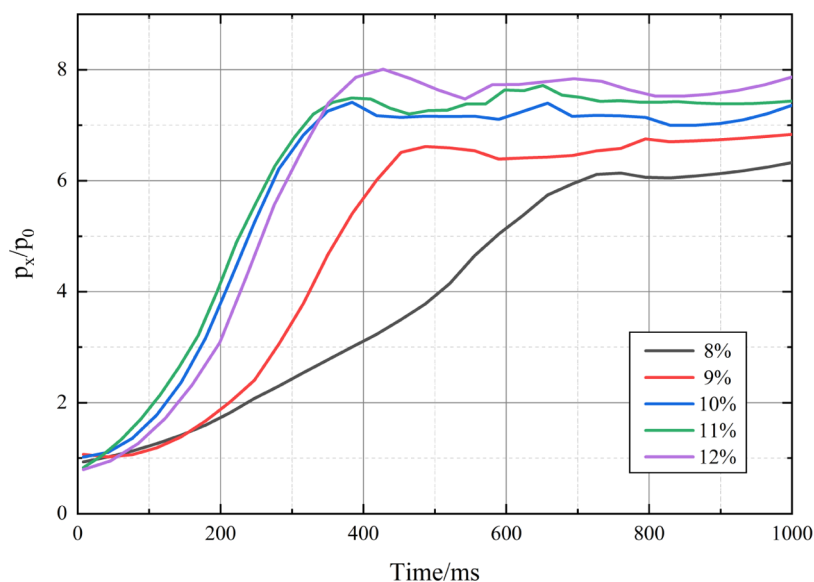
Figure 22. Variation law of the ratio of the explosion pressure to the initial pressure with different concentration gradients.
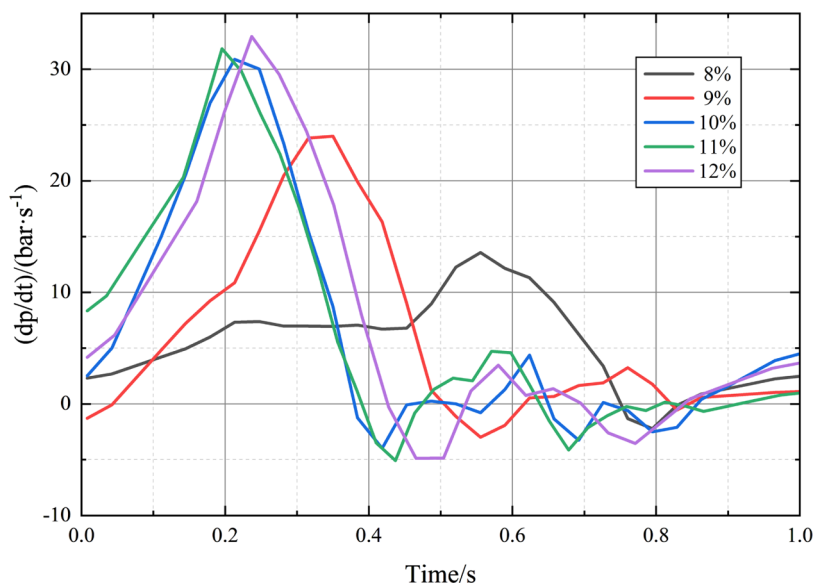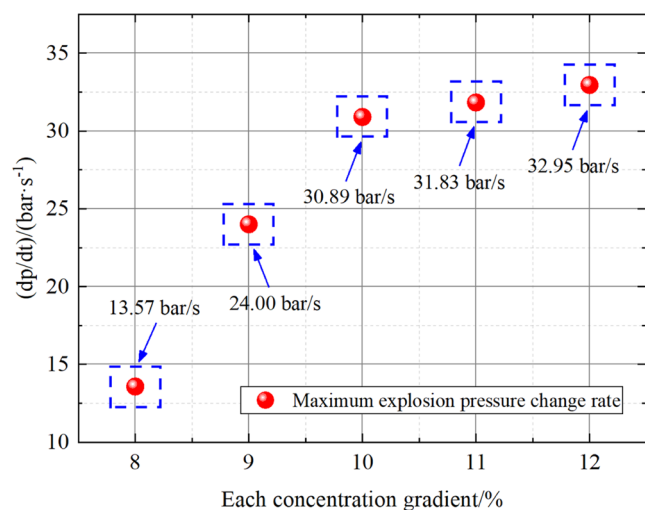

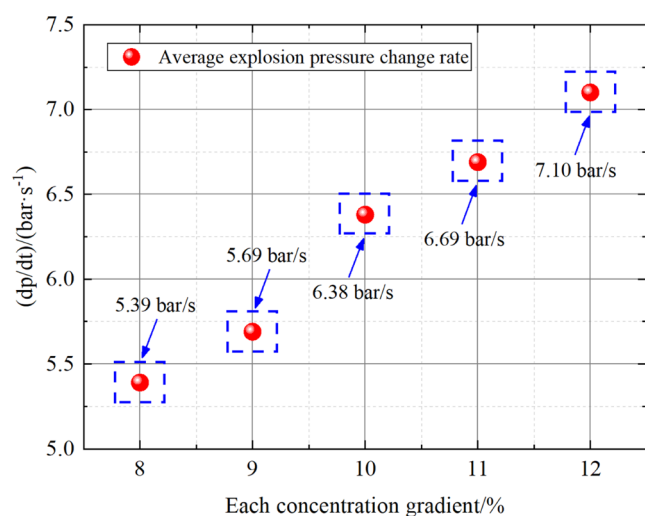**Figure 23.** Explosion pressure change rate at different concentration gradients.

The ratio relationship between the explosion pressure of different concentration gradients and the initial atmospheric pressure can be seen in Figure 22. In the figure, p_x is the pressure value at a certain moment, and p_0 is the initial atmospheric pressure of 101,325 Pa. The relationship between the concentration gradient and pressure can be seen in Figure 22. When the initial concentration increased from 10% to 11 and 12%, the peak pressure increased with the increase in concentration; when it decreased to 9 and 8%, the peak pressure decreased with the decrease in concentration. This phenomenon can be explained by the higher initial concentration of the non-uniform gas−air mixture containing a higher overall concentration of gas, and the overall amount of gas that can participate in combustion is more, making the gas explosion's pressure higher. Ultimately, it can be attributed to the fact that the peak value of the explosion pressure increases with the increase of the overall gas concentration.

In general, the concentration gradient affects the explosion pressure, and the different concentration gradients of the non-uniform gas−air mixture affect the growth rate and peak value of the explosion pressure. When the initial concentration is 10% and above, the growth rate of the explosion pressure is higher, the time to reach the peak is shorter, and the peak value of the explosion pressure increases with the increase of the concentration. When the initial concentration is lower than 10%, the growth rate of the explosion pressure decreases continuously with the decrease of the concentration, the time to reach the peak becomes longer, and the peak value of the explosion pressure also decreases continuously with the decrease of the concentration.

The rate of change of explosion pressure with different concentration gradients is shown in Figure 23. When the initial concentration is 10% and above, the pressure change rate increases continuously in the first 0.2 s, then the change rate decreases, and finally, the pressure change rate becomes close to

Figure 24. Maximum explosion pressure change rate at different concentration gradients.

Figure 25. Average explosion pressure change rate at different concentration gradients.

0 after 0.4 s; the explosion pressure remains stable. When it is reduced to 9 and 8%, the change rate of explosion pressure decreases continuously with the decrease of concentration, the time to reach the peak value also becomes longer, and finally, the rate of change of pressure tends to 0. This phenomenon is explained by the fact that the change rate of explosion pressure is related to different concentration gradients, but in the later stage of the reaction, the explosion pressures of different concentration gradients tend to be stable, making the final pressure change rate close to 0.

Meanwhile, the maximum explosion pressure change rate and the average explosion pressure change rate at different concentration gradients are shown in Figures 24 and 25. It can be seen that with the increase of the initial concentration, the overall concentration of gas increases continuously and the intensity of the explosion reaction increases, which makes the change rate of the maximum and average explosion pressure increase continuously. Therefore, it can be concluded that both the maximum and average explosion pressure change rates increase with increasing initial concentration.

5. CONCLUSIONS

The paper investigates the characteristics of the explosions of a non-uniform gas−air mixture with a concentration gradient in the roadway using the OpenFOAM code. The analysis examines the influence of fundamental model parameters, including pressure, temperature, flame speed, and pressure change law, on the explosion characteristics. By comparing explosions of a gas−air mixture gas with uniform concentrations to those with a non-uniform gas−air mixture exhibiting different concentration gradients, this study investigates the pressure, flame speed, shock wave, and other features resulting from non-uniform gas explosions under various conditions and draws the following conclusions.

(1) The presence of a concentration gradient in the non-uniform gas−air mixture leads to an elongated flame shape and increased surface area, resulting in a significantly higher flame propagation velocity compared to the uniform flame. Additionally, the concentration gradient accelerates the growth rate of the explosion pressure in the non-uniform gas−air mixture compared to the uniform gas−air mixture. However, since the overall gas concentration is the same for both cases, the magnitude of the pressure peak remains unchanged.

(2) When a non-uniform gas−air mixture with an initial concentration of 10% explodes, the flame velocity initially increases and then decreases due to the reflected shock wave compressing the flame. The density of the compressed mixture and the flame surface area increase so that the flame velocity increases again and reaches a peak value. Then, the velocity decreases and finally levels off. Overall, the flame velocity in the high-concentration area is higher than that in the low-concentration area. When the non-uniform gas−air mixture with different concentration gradient explodes, the flame velocity is different. When the initial volume concentration is 10%, the flame propagation velocity and peak velocity are the highest, but the increase and decrease of the concentration reduce the propagation and peak velocity.

(3) The explosion pressure of non-uniform gas−air mixtures with different concentration gradients has similar changing rules, and they all follow a pattern of initial increase followed by stabilization. But when the initial concentration is 10% and above, the growth rate of explosion pressure is higher, and the time to reach the peak is shorter. When the initial concentration is lower than 10%, the growth rate of the explosion pressure decreases continuously with the decrease of the concentration, and the time to reach the peak becomes longer. The higher the initial concentration, the higher the peak value of the explosion pressure. At the same time, both the maximum and average explosion pressure change rates increase with increasing initial concentration.

■ AUTHOR INFORMATION

Corresponding Author

Ke Gao − *College of Safety Science and Engineering, Liaoning Technical University, Huludao 125105, China; Key Laboratory of Mine Thermodynamic Disasters and Control of Ministry of Education, Liaoning Technical University, Huludao 125105, China*; Email: gaoke@lntu.edu.cn

Authors

Aobo Yang − *College of Safety Science and Engineering, Liaoning Technical University, Huludao 125105, China; Key Laboratory of Mine Thermodynamic Disasters and Control of Ministry of Education, Liaoning Technical University, Huludao 125105, China;* ⊙ orcid.org/0009-0008-2233-7743

Yujiao Liu − *College of Safety Science and Engineering, Liaoning Technical University, Huludao 125105, China; Key Laboratory of Mine Thermodynamic Disasters and Control of Ministry of Education, Liaoning Technical University, Huludao 125105, China*

Runzhi Li − *College of Safety and Environmental Engineering, Shandong University of Science and Technology, Qingdao 266590, China;* ⊙ orcid.org/0000-0002-4159-3215

Qiwen Li − *College of Safety Science and Engineering, Liaoning Technical University, Huludao 125105, China; Key Laboratory of Mine Thermodynamic Disasters and Control of Ministry of Education, Liaoning Technical University, Huludao 125105, China*

Shengnan Li − *College of Safety Science and Engineering, Liaoning Technical University, Huludao 125105, China; Department of Mechanical Engineering, National University of Singapore, Singapore 117576, Republic of Singapore;* ⊙ orcid.org/0000-0002-9046-388X

Complete contact information is available at:
https://pubs.acs.org/10.1021/acsomega.3c06054

Author Contributions

[⊥]A.Y. and Y.L. contributed equally to this work.

Notes

The authors declare no competing financial interest.

■ REFERENCES

(1) Li, X.; Chen, H.; Li, H.; Chen, J. Change Law of Lower Limit of Gas Explosion at Ultra-High Temperatures. *ACS Omega* **2021**, *6*, 35112−35123.

(2) Zhang, X.; Wang, H.; Yang, M.; Han, L.; Wang, P. Application of a Simulation Method for the Shock Wave Propagation Law of Gas Explosion. *ACS Omega* **2022**, *7*, 31049−31058.

(3) Li, C.; Qiao, Z.; Hao, M.; Zhang, H.; Li, G. Effect of Ignition Energy on Environmental Parameters of Gas Explosion in Semiclosed Pipeline. *ACS Omega* **2022**, *7*, 10394−10405.

(4) Jia, H.; Cui, B.; Duan, Y.; Zheng, K. Study on the Influence of Vent Shape and Blockage Ratio on the Premixed Gas Explosion in the Chamber with a Small Aspect Ratio. *ACS Omega* **2022**, *7*, 22787−22796.

(5) Oppenheim, A. K.; Soloukhin, R. I. Experiments in gasdynamics of explosions. *Annu. Rev. Fluid Mech.* **1973**, *5*, 31−58.

(6) Lee, J. H. S.; Moen, I. O. The mechans of transition from deflagration to detonation in vapor cloud explosions. *Prog. Energy Combust. Sci.* **1980**, *6*, 359−389.

(7) Cai, P.; Liu, Z.; Li, M.; Zhao, Y.; Li, P.; Li, S.; Li, Y. Experimental study of effect of equivalence ratio and initial turbulence on the explosion characteristics of LPG/DME clean blended fuel. *Energy* **2022**, *250*, No. 123858.

(8) Gelfand, B. E.; Frolov, S. M.; Nettleton, M. A. Gaseous detonations-a selective review. *Prog. Energy Combust. Sci.* **1991**, *17*, 327−371.

(9) Oran, E. S.; Gamezo, V. N. Origins of the deflagration-to-detonation transition in gas-phase combustion. *Combust. Flame* **2007**, *148*, 4−47.

(10) Gao, K.; Li, S.; Han, R.; Li, R.; Liu, Z.; Qi, Z.; Liu, Z. Study on the propagation law of gas explosion in the space based on the goaf characteristic of coal mine. *Saf. Sci.* **2020**, *127*, No. 104693.

(11) Zhang, Q.; Ma, Q. J. Dynamic pressure induced by a methane−air explosion in a coal mine. *Process Saf. Environ. Prot.* **2015**, *93*, 233−239.

(12) Gao, K.; Liu, Z.; Wu, C.; Li, J.; Liu, K.; Liu, Y.; Li, S. Effect of low gas concentration in underground return tunnels on characteristics of gas explosions. *Process Saf. Environ. Prot.* **2021**, *152*, 679−691.

(13) Wang, K.; Jiang, S.; Ma, X.; Wu, Z.; Zhang, W.; Shao, H. Study of the destruction of ventilation systems in coal mines due to gas explosions. *Powder Technol.* **2015**, *286*, 401−411.

(14) Zhou, Y.; Li, Y.; Jiang, H.; Zhang, K.; Chen, X.; Huang, L.; Gao, W. Investigations on unconfined large-scale methane explosion with the effects of scale and obstacles. *Process Saf. Environ. Prot.* **2021**, *155*, 1−10.

(15) Cao, M.; Zhang, Y.; Li, R.; Chen, X.; Zhang, M.; Dong, H. Explosion and vented explosion behaviors of low-concentration gas in large-scale pipes. *Eng. Sci. Technol.* **2023**, *42*, No. 101410.

(16) Yang, S.; Sun, W.; Fang, Q.; Yang, Y.; Xia, C.; Bao, Q. Investigation of a practical load model for a natural gas explosion in an unconfined space. *J. Saf. Sci. Resil.* **2022**, *3*, 209−221.

(17) Xu, J.; Liu, Y.; Chen, X.; Li, D.; Liu, J.; Zhang, Y. Effects of equivalent ratio of methane to air mass concentration on flame structure and propagation characteristics. *China Saf. Sci. J.* **2014**, *24*, 64−69.

(18) Cheng, J.; Zhang, B.; Liu, H.; Wang, F. The precursor shock wave and flame propagation enhancement by CO2 injection in a methane-oxygen mixture. *Fuel* **2021**, *283*, No. 118917.

(19) Wei, C.; Tan, Y. Experimental study on the propagation characteristics of methane explosion with different concentrations in the pipeline. *Saf. Coal Mines* **2009**, *40*, 4−6.

(20) Song, C. *Research on the Effect of Gas Concentration on Pipeline Explosion Propagation*; Inner Mongolia Coal Economy, 2017; Vol. 7; pp 144−145.

(21) Li, R.; Si, R. Effect of gas concentration on explosion pressure and pressure rise rate. *J. Xi'an Univ. Sci. Technol.* **2010**, *30*, 29−33.

(22) Rui, S.; Wang, C.; Guo, S.; Jing, R.; Li, Q. Hydrogen-air explosion with concentration gradients in a cubic enclosure. *Process Saf. Environ. Prot.* **2021**, *151*, 141−150.

(23) Huang, C.; Chen, X.; Liu, L.; Zhang, H.; Yuan, B.; Li, Y. The influence of opening shape of obstacles on explosion characteristics of premixed methane-air with concentration gradients. *Process Saf. Environ. Prot.* **2021**, *150*, 305−313.

(24) Wang, C. J.; Wen, J. X. Numerical simulation of flame acceleration and deflagration-to-detonation transition in hydrogen-air mixtures with concentration gradients. *Int. J. Hydrogen Energy* **2017**, *42*, 7657−7663.

(25) Karanam, A.; Sharma, P. K.; Ganju, S. Numerical simulation and validation of flame acceleration and DDT in hydrogen air mixtures. *Int. J. Hydrogen Energy* **2018**, *43*, 17492−17504.

(26) Zhang, B.; Li, Y.; Liu, H. Analysis of the ignition induced by shock wave focusing equipped with conical and hemispherical reflectors. *Combust. Flame* **2022**, *236*, No. 111763.

(27) Zhang, B.; Li, Y.; Liu, H. Ignition behavior and the onset of quasi-detonation in methane-oxygen using different end wall reflectors. *Aerosp. Sci. Technol.* **2021**, *116*, No. 106873.

(28) Yang, Z.; Cheng, J.; Zhang, B. Deflagration and detonation induced by shock wave focusing at different Mach numbers. *Chin. J. Aeronaut.* **2023**, No. 29, DOI: 10.1016/j.cja.2023.06.029.

(29) Cao, W.; Li, W.; Zhang, L.; Chen, J.; Yu, S.; Zhou, Z.; Zhang, Y.; Shen, X.; Tan, Y. Flame characteristics of premixed H2-air mixtures explosion venting in a spherical container through a duct. *Int. J. Hydrogen Energy* **2021**, *46*, 26693−26707.

(30) Cao, W.; Li, W.; Zhang, Y.; Zhou, Z.; Zhao, Y.; Yang, Z.; Liu, X.; Yu, S.; Tan, Y. Experimental study on the explosion behaviors of

premixed syngas-air mixtures in ducts. *Int. J. Hydrogen Energy* **2021**, *46*, 23053−23066.

(31) Zhang, L.; Wang, H.; Chen, C.; Wang, P.; Xu, L. Experimental study to assess the explosion hazard of CH_4/coal dust mixtures induced by high-temperature source surface. *Process Saf. Environ. Prot.* **2021**, *154*, 60−71.

(32) Bi, M.; Dong, C.; Zhou, Y. Numerical simulation of premixed methane−air deflagration in large L/D closed pipes. *Appl. Therm. Eng.* **2012**, *40*, 337−342.

(33) Bai, C.; Chang, X.; Zhang, B. Impacts of turbulence on explosion characteristics of methane-air mixtures with different fuel concentration. *Fuel* **2020**, *271*, No. 117610.

(34) Ciccarelli, G.; Dorofeev, S. Flame acceleration and transition to detonation in ducts. *Prog. Energy Combust. Sci.* **2008**, *34*, 499−550.

(35) Azadboni, R. K.; Heidari, A.; Wen, J. X. Numerical studies of flame acceleration and onset of detonation in homogenous and inhomogeneous mixture. *J. Loss Prev. Process Ind.* **2020**, *64*, No. 104063.

(36) Ettner, F.; Vollmer, K. G.; Sattelmayer, T. Numerical simulation of the deflagration-to-detonation transition in inhomogeneous mixtures. *J. Combust.* **2014**, *2014*, No. 686347, DOI: 10.1155/2014/686347.

(37) Han, W.; Gao, Y.; Law, C. K. Flame acceleration and deflagration-to-detonation transition in micro-and macro-channels: An integrated mechanistic study. *Combust. Flame* **2017**, *176*, 285−298.

(38) Launder, B. E.; Spalding, D. B. The Numerical Computation of Turbulent Flows. In *Numerical Prediction of Flow, Heat Transfer, Turbulence and Combustion*; Launder, B. E.; Spalding, D. B., Eds.; Pergamon, 1983; pp 96−116.

(39) Cengel, Y. A.; Ghajar, A. J. *Heat and Mass Transfer*, 4th ed.; Tata McGraw Hill Education, 2011.

(40) Agrawal, N.; Velusamy, K.; Das, S. K. A study on the scaling features for mixing and deflagration potential of stratified layer of hydrogen due to molecular diffusion. *Int. Commun. Heat Mass Transfer* **2013**, *48*, 28−33.

(41) Cowie, M.; Watts, H. Diffusion of methane and chloromethanes in air. *Can. J. Chem.* **1971**, *49*, 74−77.

(42) Shamsadin Saeid, M. H.; Khadem, J.; Emami, S.; Ghodrat, M. Effect of diffusion time on the mechanism of deflagration to detonation transition in an inhomogeneous mixture of hydrogen-air. *Int. J. Hydrogen Energy* **2022**, *47*, 23411−23426.